Atmos. Chem. Phys. Discuss., 8, 18727–18764, 2008
www.atmos-chem-phys-discuss.net/8/18727/2008/
© Author(s) 2008. This work is distributed under
the Creative Commons Attribution 3.0 License.

Atmospheric Chemistry and Physics Discussions

This discussion paper is/has been under review for the journal *Atmospheric Chemistry and Physics (ACP)*. Please refer to the corresponding final paper in *ACP* if available.

Implications of Lagrangian transport for coupled chemistry-climate simulations

A. Stenke[1], **M. Dameris**[1], **V. Grewe**[1], **and H. Garny**[2]

[1]Deutsches Zentrum für Luft- und Raumfahrt (DLR), Institut für Physik der Atmosphäre, Oberpfaffenhofen, Germany
[2]Meteorological Institute, University of Munich, Munich, Germany

Received: 4 July 2008 – Accepted: 14 September 2008 – Published: 31 October 2008

Correspondence to: A. Stenke (andrea.stenke@dlr.de)

Published by Copernicus Publications on behalf of the European Geosciences Union.

Abstract

For the first time a purely Lagrangian transport algorithm is applied in a fully coupled chemistry-climate model (CCM). We use the Lagrangian scheme ATTILA for the transport of water vapour, cloud water and chemical trace species in the ECHAM4.L39(DLR)/CHEM (E39C) CCM. The advantage of the Lagrangian approach is that it is numerically non-diffusive and therefore maintains steeper and more realistic gradients than the operational semi-Lagrangian transport scheme. In case of radiatively active species changes in the simulated distributions feed back to model dynamics which in turn affect the modelled transport. The implications of the Lagrangian transport scheme for stratospheric model dynamics and tracer distributions in the upgraded model version E39C-ATTILA (E39C-A) are evaluated by comparison with observations and results of the E39C model with the operational semi-Lagrangian advection scheme. We find that several deficiencies in stratospheric dynamics in E39C seem to originate from a pronounced modelled wet bias and an associated cold bias in the extra-tropical lowermost stratosphere. The reduction of the simulated moisture and temperature bias in E39C-A leads to a significant advancement of stratospheric dynamics in terms of the mean state as well as annual and interannual variability. As a consequence of the favourable numerical characteristics of the Lagrangian transport scheme and the improved model dynamics, E39C-A generally shows more realistic stratospheric tracer distributions: Compared to E39C high stratospheric chlorine (Cl_y) concentrations extend further downward and agree now well with analyses derived from observations. Therefore E39C-A realistically covers the altitude of maximum ozone depletion in the stratosphere. The location of the ozonopause, i.e. the transition from low tropospheric to high stratospheric ozone values, is also clearly improved in E39C-A. Furthermore, the simulated temporal evolution of stratospheric Cl_y in the past is realistically reproduced which is an important step towards a more reliable projection of future changes, especially of stratospheric ozone.

ACPD

8, 18727–18764, 2008

1 Introduction

Coupled chemistry-climate models (CCMs) are a common tool to study past changes and to predict the future evolution of the stratosphere. Assessing the reliability of those model predictions requires a detailed knowledge on the capabilities and limitations of the applied models. For this purpose different generations of CCMs and their underlying general circulation models (GCMs) are reviewed periodically in various model intercomparison projects (e.g. Park et al., 1999; Gates et al., 1999; Pawson et al., 2000; Austin et al., 2003). In a recent model intercomparison (Eyring et al., 2006) the performance of thirteen CCMs has been evaluated against observations with a special focus on quantities that are important for simulating the evolution of ozone and ozone recovery. The participating models covered a great bandwidth of different model formulations, e.g. with respect to the underlying GCMs, transport algorithms, chemistry schemes or the model domain and resolution. Depending on the evaluated quantity the models showed more or less agreement among each other or with observations. For example, most models showed a temperature bias in the extra-tropical lowermost stratosphere, but the simulated stratospheric temperature trend over the period between 1960 and 2000 was in fairly good agreement with observations. A large inter-model spread, however, was obvious in the simulated tracer distributions like those of methane or inorganic chlorine (Cl_y), indicating large differences in transport. This kind of model evaluation can provide useful insights in model deficiencies and general uncertainties in our understanding of mechanisms and feedback processes. For the identification of causes of model shortcomings a more detailed analysis of model results and sensitivity simulations with respect to individual parameterisations are necessary.

One of the participating models was the CCM ECHAM4.L39(DLR)/CHEM (E39C) (Dameris et al., 2005). The model evaluation of Eyring et al. (2006) summarised various shortcomings in E39C with respect to model dynamics and tracer distributions. Like most of the models, E39C exhibits a severe temperature bias in the extra-tropical

ACPD
8, 18727–18764, 2008

lowermost stratosphere (cold bias) as well as in polar regions in the model top layers (see also Dameris et al., 2005). The stratospheric temperature errors have further implications for model dynamics like a delayed break down of the polar vortex. Furthermore, the comparison with observations indicated biases in simulated tracer fields which might be caused by deficiencies in model dynamics as well as limitations of the applied transport algorithm. For example, the atmospheric tape recorder signal in E39C indicates a too rapid upward propagation in the tropics. E39C also has problems simulating the stratospheric methane distribution or stratospheric Cl_y trends. The latter has an impact on simulated ozone trends which are too weak in E39C. The exact cause and effect relationships causing these model deficiencies are generally not obvious and figuring them out is often challenging. Compared to the other participating models E39C has the lowest vertical resolution above 50 hPa, with the uppermost model level being centred at 10 hPa. Thus E39C deficiencies are often simply attributed to the low model top.

A first important step towards a significant improvement of model dynamics has been done in a recent study of Stenke et al. (2007) employing the fully Lagrangian, numerically non-diffusive, and strictly mass conserving advection scheme ATTILA (Reithmeier and Sausen, 2002) for the transport of water vapour and cloud water in the ECHAM4.L39(DLR) GCM (without coupled chemistry). In the operational version (e.g. Roeckner et al., 1996; Land et al., 2002) a semi-Lagrangian advection scheme is used for tracer transport which exhibits an exceptional high numerical diffusion in the presence of sharp tracer gradients. In case of water vapour this leads to an artificial horizontal diffusion of water vapour from the tropical upper troposphere into the extra-tropical lowermost stratosphere and a severe overestimation of water vapour within this atmospheric region (wet bias). In turn, the simulated wet bias contributes to a cold bias in the extra-tropical lowermost stratosphere due to excessive longwave cooling rates. The use of ATTILA results in a pronounced and consistent reduction of the modelled biases, e.g. the cold bias in the extra-tropical lowermost stratosphere is reduced to one third of its original amount. The advancements in simulated temperatures have a

ACPD
8, 18727–18764, 2008

remarkable impact on model dynamics, e.g. on the representation of the extra-tropical tropopause or the zonal winds in the stratosphere.

In the present study the Lagrangian approach described in Stenke et al. (2007) has been extended to chemical trace species. According to our knowledge this is the first time that a purely Lagrangian advection scheme is used for the transport of active trace species in a global, interactively coupled CCM. Concerning chemistry modelling Lagrangian methods have been applied in chemistry transport models (CTMs) like STOCHEM (Collins et al., 2000, and references therein), GRANTOUR (e.g. Atherton et al., 1996) or CLAMS (McKenna et al., 2002a,b) exclusively, with encouraging results. Furthermore, in a few cases Lagrangian schemes have been used in GCMs for the transport of passive trace species (e.g. Eluszkiewicz et al., 2000; Reithmeier and Sausen, 2002). Here we present an upgraded model version of the coupled chemistry-climate model E39C employing the Lagrangian advection scheme ATTILA for water vapour, cloud water as well as all chemical trace species, i.e. E39C-A. The intention of this paper is to evaluate the performance of this new model version and to document significant improvements with regard to model dynamics and simulated tracer distributions, but also to identify remaining model deficiencies that cannot be cured by a superior transport algorithm. Like the evaluation of Eyring et al. (2006), the study is based on a transient model simulation of the year 1960 to 2004 including several anthropogenic and natural forcings.

In the following section E39C-A as well as the experimental set-up of the performed model simulation are briefly described. Several advancements in model dynamics have already been discussed in Stenke et al. (2007) and are shortly summarised in Sect. 3.1. Sections 3.2 and 3.3 focus on model improvements with regard to stratospheric transport and tracer distributions. A summary and concluding remarks are given in Sect. 4.

ACPD
8, 18727–18764, 2008

2 Model description and experimental set-up

2.1 The CCM ECHAM4.L39(DLR)/CHEM/ATTILA

In this study, we use the coupled chemistry-climate model ECHAM4.L39(DLR)/CHEM/-ATTILA (hereafter referred to a E39C-A) which is an upgraded version of the CCM ECHAM4.L39(DLR)/CHEM (E39C) (Dameris et al., 2005) employing the fully Lagrangian advection scheme ATTILA (Reithmeier and Sausen, 2002) for tracer transport. The model system E39C (Hein et al., 2001) has been applied for several chemistry-climate studies based on time-slice (e.g. Schnadt et al., 2002; Grewe et al., 2004; Stenke and Grewe, 2005) as well as transient simulations (Dameris et al., 2005, 2006; Grewe, 2007).

E39C consists of the dynamic part E39 and the chemistry module CHEM. E39 is a spectral general circulation model, based on the climate model ECHAM4 (Roeckner et al., 1996), and has a vertical resolution of 39 levels up to the top layer centred at 10 hPa (Land et al., 2002). In the uppermost model layers ("sponge layer") horizontal diffusion is gradually enhanced to prevent spurious wave reflection at the model top. These numerical requirements yield a suppressed model variability in the 2 uppermost layers, i.e. above 25 hPa. A spectral horizontal resolution of T30 ($\approx 6^\circ$ isotropic resolution) is used in this study. The corresponding Gaussian transform grid, on which the tracer transport, model physics and chemistry are calculated, has a mesh size of approximately $3.75^\circ \times 3.75^\circ$. The chosen time step is 24 min.

The chemistry module CHEM (Steil et al., 1998) is based on the family concept. It includes stratospheric homogeneous and heterogeneous ozone chemistry and the most relevant chemical processes for describing the tropospheric background chemistry with 107 photochemical reactions, 37 chemical species and 4 heterogeneous reactions on polar stratospheric clouds (PSCs) and on sulphate aerosols. In addition to E39C the present model version includes a parameterisation for bromine chemistry (ClO/BrO-cycle) based on the photolysis of Cl_2O_2 (based on Rex et al., 2003). To account for the effects of twilight stratospheric ozone chemistry the photolysis at solar zenith angles

CC BY

up to 93° has been implemented (Lamago et al., 2003). Net heating rates and photolysis rates are calculated on-line from the modelled distributions of the radiatively active gases O_3, CH_4, N_2O, H_2O and CFCs, and the actual cloud distribution. NO_x emissions from lightning are parameterised according to the approach developed by Grewe et al. (2001) who related the flash rate to the vertical mass flux within a convective cloud. The annual mean emission rate of lightning NO_x amounts to 5.36 Tg(N)/a.

Water vapour, cloud water and chemical trace species are advected by the Lagrangian advection scheme ATTILA (Reithmeier and Sausen, 2002) instead of the operational semi-Lagrangian advection scheme of Williamson and Rasch (1994) which has been used in the previous model version E39C. Since the semi-Lagrangian scheme itself is not mass conserving, a mass fixer has to be applied which is an integral part of the scheme (Rasch and Williamson, 1990). In contrast, the purely Lagrangian scheme ATTILA is strictly mass conserving and numerically non-diffusive. Transport studies with the ECHAM4 GCM using passive tracers have shown that ATTILA is able to maintain steeper and more realistic gradients than the semi-Lagrangian scheme (Reithmeier and Sausen, 2002). Furthermore, the simulated age of air in ECHAM4 strongly depends on the advection scheme, with ATTILA producing the older and more realistic ages (Land et al., 2002; Reithmeier et al., 2008). This agrees well with findings of Eluszkiewicz et al. (2000) that the most realistic results in terms of age of air are obtained with non-diffusive schemes.

To cope with the applied spatial resolution (T30, 39 vertical levels) the mass of the model atmosphere is divided into approximately 500 000 air parcels of equal mass which are advected three-dimensionally using the actual model wind field. ATTILA includes state-of-the-art parameterisations of convective transport, mixing due to inter-parcel exchange, and boundary layer turbulence which are described comprehensively by Reithmeier and Sausen (2002).

Reithmeier and Sausen (2002) applied ATTILA for the transport of passive tracers exclusively. In a recent study of Stenke et al. (2007), ATTILA has been extended successfully to water vapour and cloud water. The treatment of active trace species re-

CC BY

quires some modifications to ATTILA concerning the mapping between air parcels and model grid. The model grid is used for the calculation of radiation, convection and other physical processes, and to handle the diagnostic output. For this purpose, the tracer concentrations are mapped from the air parcels to the ECHAM model grid by averaging the tracer concentrations of all air parcels within the same grid box. Since the radiation scheme requires complete tracer fields, a suitable algorithm is used to "fill" empty grid boxes, i.e. a reasonable tracer concentration is assigned to the respective grid box. A detailed description of the applied approach is given in Stenke et al. (2007).

In the present study the concept described in Stenke et al. (2007) has been adopted for the transport of chemical trace species. While in case of water vapour and cloud water the tracer content on the Lagrangian air parcels is given as mass mixing ratios, volume mixing ratios are used in case of the chemical trace species.

2.2 Experimental set-up

The present study is based on a transient simulation designed to represent the atmospheric development from 1960 to 2004. Therefore, as many as possible natural and anthropogenic forcings are included, like the 11-year solar cycle, the QBO, chemical and direct radiative effects of major volcanic eruptions, the increase in well mixed greenhouse gas concentrations and surface NO_x emissions. The model design mainly follows the description given in Dameris et al. (2005). In the following, the experimental set-up and modifications compared to Dameris et al. (2005) are briefly summarised. After a 10-year spin-up with stationary conditions of the late 1950s the model has been integrated from 1960 to 2004 using transient boundary conditions.

The SSTs are given as monthly means following the global sea ice and sea surface temperature data set HadISST1 provided by the UK Met Office Hadley Center (Rayner et al., 2003, available via http://hadobs.org/). The data set is based on blended satellite and in situ observations.

Both, chemical and direct radiative effects of enhanced stratospheric aerosol abundance from the three major volcanic eruptions of Agung (1963), El Chichón (1982)

CC BY

and Mount Pinatubo (1991) are taken into account. For the heterogeneous reactions covered in the chemistry module, observed sulphate aerosol surface area densities (SADs) are prescribed as monthly means. The SADs have been deduced from satellite data, as described in Jackman et al. (1996) and updated by D. B. Considine (NASA Langley Research Center). This data set covers the period from 1979 to 1999. For the years before 1979 SADs have been calculated as described in Dameris et al. (2005), and for the period 2000–2004 the mean value of the years 1997 to 1999 has been used.

Eruption-related radiative heating is implemented using additional monthly and zonal mean net heating rates. The heating rates mark a modification to the model set up described in Dameris et al. (2005) who used a data set provided by Kirchner et al. (1999). The heating rates applied in the present study were calculated by G. Stenchikov and L. Oman using volcanic aerosol parameters from Sato et al. (1993), Hansen et al. (2002) and GISS Model E radiative routines and climatology (Schmidt et al., 2006, for further information see http://www.pa.op.dlr.de/CCMVal/Forcings/CCMVal_Forcings.html). This data set covers the years from 1950 to 1999. For the years 2000 to 2004 the values of 1999 have been used. In tropical regions the updated volcanic heating rates are generally smaller than in the data set of Kirchner et al. (1999). In polar regions of the lower stratosphere the new data set shows a substantial radiative cooling for 2–3 years after a volcanic eruption which was not apparent in the data set of Kirchner et al. (1999).

The QBO is forced externally by a linear relaxation ("nudging") of the simulated zonal winds in the equatorial stratosphere to a constructed QBO time series which follows observed equatorial zonal wind profiles (Giorgetta and Bengtsson, 1999). This assimilation is applied equatorwards of 20° latitude from 90 hPa up to the model top layer. The relaxation time scale is set uniformly to 7 days within the QBO core domain above 50 hPa and between 10° N and 10° S. Outside the core region the relaxation time depends on latitude and pressure (Giorgetta and Bengtsson, 1999).

The influence of the 11-year solar cycle on photolysis is parameterised according to

CC BY

the intensity of the 10.7 cm radiation of the sun (Lean et al., 1997, data available via http://www.drao.nrc.ca/icarus/www/daily.html). The impact of solar activity on shortwave radiative heating rates is considered on the basis of changes of the solar constant (Dameris et al., 2005, their Table 2).

The temporal development of the mixing ratios of the most relevant greenhouse gases (CO_2, N_2O, CH_4) is based on IPCC (2001). CO_2 is prescribed for the entire model domain, the others at the surface according to Hein et al. (1997). Nitrogen oxide (NO_x=NO+NO_2) emissions from several natural (lightning, biomass burning, soils) and anthrogopenic (industry, aircraft, ships, surface transportation) sources are considered in the model simulation. NO_x emissions from lightning (Sect. 2.1), soils, ships and aircraft follows the description in Dameris et al. (2005). NO_x emissions from industry, biomass burning and surface transportation are based on the RETRO emission inventory which means another modification to the model set up in Dameris et al. (2005). A detailed description of the RETRO data set can be found in RETRO (2007, report available via http://retro.enes.org/pub_reports.shtml)

To account for exchange processes from the upper stratosphere, boundary conditions for the two families Cl_x and NO_y are prescribed at the uppermost model level (10 hPa). Monthly mean concentrations are taken from the two-dimensional middle atmosphere model by Brühl and Crutzen (1993) which also includes effects from the 11-year solar cycle. Since chlorofluorocarbons (CFCs) are not explicitly transported in E39C-A, two-dimensional distributions (depending on latitude and altitude) based on the results from the model by Brühl and Crutzen (1993) are prescribed. The temporal development of CFC concentrations is in agreement with the assumptions made in WMO (2003).

3 Results

Using the Lagrangian advection scheme in E39C-A leads to tracer distributions different from those in E39C. In a fully coupled CCM these changes modify radiative heating

CC BY

rates and, eventually, model dynamics. The study of Stenke et al. (2007) has shown how the improvements with respect to the simulated water vapour distribution arising from the use of ATTILA directly feed back to modelled temperatures and other dynamic variables. In the following we will assess the impact of the new Lagrangian advection scheme ATTILA on tracer distributions and model dynamics in E39C-A, with a special focus on the stratosphere. Another important question is how changes in the mean model climate and mean tracer distributions affect simulated long-term changes and variability. This aspect is of particular interest in view of reliable estimates of future changes.

3.1 Stratospheric dynamics

Stenke et al. (2007) have reported obvious improvements regarding model dynamics in response to the reduced wet and cold bias in the extra-tropical lowermost stratosphere. For example, the simulated tropopause characteristics in E39/ATTILA (hereafter referred to E39-A) are in better agreement with respective ERA40 data, in particular in extra-tropical regions where the simulated tropopause is clearly shifted downward (cp. Fig. 10 in Stenke et al., 2007). The climatological mean zonal wind fields for solstice conditions are improved with regard to ERA40 re-analyses (Uppala et al., 2005). The strength of the polar night jets is slightly reduced (e.g. by about 5 m/s in the Southern Hemisphere), but still stronger than observed. The most obvious upgrade is found during summer months with both hemispheres showing a much better representation of the downward propagation of the zero wind line into the lower stratosphere, i.e. the transition from westerlies to easterlies between November and January in the Southern Hemisphere and between June and August in the Northern Hemisphere (cp. Fig. 11 in Stenke et al., 2007). Both, the CCM E39C and the underlying GCM E39 are not able to simulate adequately the observed wind reversal in the stratosphere below 10 hPa in a realistic manner, especially in the Southern Hemisphere (Dameris et al., 2005).

The upgrades of E39-A are also visible in the mean annual cycle of both, the zonal mean wind and temperature in the lower stratosphere (cp. Fig. 12 in Stenke et al.,

ACPD
8, 18727–18764, 2008

2007). Moreover, it is worth mentioning that the interannual variability is enhanced during Northern Hemisphere winter season, particularly in early winter months which is in better agreement with observations. All these improvements of stratospheric dynamics apparent in time slice simulations with E39-A are also found in the transient simulation with E39C-A and therefore will not be presented again. In the following we will concentrate on consequent advancements in interactions between planetary waves and the mean flow in terms of Eliassen-Palm (EP) fluxes and the meridional heat flux. Wave propagation and dissipation are key drivers of stratospheric transport and variability, and it is important to reasonably simulate the impact of changes in wave activity on stratospheric dynamics and therefore on the future evolution of stratospheric ozone (a key objective when using CCMs).

Both, EP fluxes and EP divergence fields during solstice conditions as simulated with E39C-A are presented in Fig. 1 for the lower stratosphere. The EP fluxes were calculated including ageostrophic terms as given in Robinson (1986, their Eq. 5) and were weighted by the mass of an annular ring (Edmon et al., 1980). The transfer of wave energy from one latitude and height to another is correctly simulated with E39C-A, showing strong upward fluxes in the winter hemispheres and turning towards lower latitudes at higher altitudes. E39C-A shows a clear difference between the summer and winter hemispheres which is not adequately captured by E39C (not shown). A reason is that the summer easterlies in the extra-tropical lower stratosphere (below 10 hPa) are only insufficiently represented by E39C and therefore planetary waves propagate higher into the summer stratosphere. The patterns of EP divergence (colour coded in Fig. 1) are associated with wave breaking processes (i.e. eddy dissipation) and represent an ideal diagnostic tool to quantify the effects of waves on the mean state. Furthermore, the mean meridional circulation in the stratosphere is largely driven by wave dissipation as quantified by EP divergence (via downward control as explained by Haynes et al., 1991). Since the mean circulation is responsible for large-scale tracer transport, deficiencies found in EP diagnostics will be reflected in simulated tracer distributions. The EP divergence fields of E39C-A calculated for solstice conditions are

ACPD
8, 18727–18764, 2008

in reasonable agreement with respective analyses from long-term reanalyses (see e.g. Hitchman and Huesmann, 2007), for example indicating a more pronounced region of EP convergence, i.e. imposing stronger westward forces, in the Northern Hemisphere winter stratosphere than in southern winter. As mentioned above, the more realistic simulation of stratospheric winds by E39C-A compared to E39C leads to changes in wave propagation. This causes EP divergences to be generally smaller in E39C-A and therefore a decreased forcing on the mean meridional circulation. The resulting change in tropical upwelling is further discussed in Sect. 3.2.1.

The second diagnostic we use to quantify the wave forcing of the stratosphere is given in terms of the meridional heat flux ($\overline{v'T'}$) at 100 hPa which is proportional to the vertical component of the EP flux entering the lower stratosphere. The correlation of heat fluxes at 100 hPa (averaged over 40° N to 80° N for January/February and 40° S to 80° S for July/August, respectively) versus temperature at 50 hPa (averaged over 60° N to 90° N for February/March and 60° S to 90° S for August/September, respectively), which was introduced by Newman et al. (2001), is used to estimate the connection between wave activity and the response of the lower stratosphere. Figure 2 compares the model results for the Southern Hemisphere with NCEP/NCAR reanalyses. Both model versions show a statistically significant (on the 95% level) flatter slope of the correlation between temperature and heat flux which indicates that the temperature response to changes in the wave forcing is underestimated. The vertical offset between model results and meteorological analyses reflects the simulated cold bias in the lower stratosphere which is clearly reduced in E39C-A. In the Northern Hemisphere (not shown, cp. Fig. 3 in Eyring et al., 2006, for E39C) both model versions E39C and E39C-A correctly reproduce the slope of the linear fit. Since the cold bias is reduced in E39C-A, the vertical displacement is again slightly reduced.

In the following sections the implications of the Lagrangian scheme for stratospheric transport and simulated tracer distributions are discussed. It should be mentioned that both, advanced numerics of the advection algorithm and improved model dynamics, contribute to changes in simulated tracer distributions.

CC BY

3.2 Stratospheric transport

The stratospheric transport characteristics of the new model version E39C-A are examined by various diagnostics which have already been presented for E39C in Eyring et al. (2006). First, the vertical ascent in the tropics as well as the tropical-midlatitude mixing are evaluated by means of the atmospheric tape recorder signal (Mote et al., 1996). Information about the downward transport inside the polar vortex are obtained from the simulated methane distribution.

3.2.1 Atmospheric tape recorder

The atmospheric tape recorder signal is triggered by the annual temperature variations at the tropical cold point tropopause. The mean annual cycle of temperatures near the tropical tropopause (100 hPa) is shown in Fig. 3 (left). To facilitate the comparison with ERA40 data the 100 hPa temperatures are used instead of the cold point temperature. E39C overestimates the ERA40 temperatures at this level by about 2–3 K, and, consequently, the observed water vapour mixing ratios by about 3 ppmv (Fig. 3 right). Furthermore, E39C overestimates the amplitude of the water vapour annual cycle by about 1 ppmv. The upgraded model version E39C-A shows much better agreement with reanalyses and observations, both in terms of absolute values (see also Stenke et al., 2007) and in terms of the seasonal variation.

The annual variations in water vapour mixing ratios at the tropical tropopause propagate upward into the tropical stratosphere which provides information about the ascent rate and the subtropical transport barrier. Figure 4 shows the time-height section of water vapour deviations averaged between 10° N and 10° S, the so-called atmospheric tape recorder, for E39C and E39C-A. HALOE observations (Grooß and Russell, 2005) are used for comparison. The amplitude of the water vapour deviations throughout the lowermost stratosphere is induced by the variations of the cold point temperature. The decay of the amplitude with height, however, is controlled by transport processes, primarily by horizontal mixing between tropics and extra-tropics. The attenuation of the

ACPD
8, 18727–18764, 2008

tape recorder signal as simulated with E39C is in reasonable agreement with HALOE observations. However, compared to HALOE the propagation time of the tape recorder signal in E39C is less than half, indicating a too fast ascent in the tropics.

From Fig. 4 it is evident that the simulated tape recorder signal in E39C-A is in much better agreement with HALOE than in E39C. E39C-A correctly reproduces the amplitude of the observed water vapour deviation in the tropical lowermost stratosphere. In the lower stratosphere also the decay of the tape recorder signal with height is in reasonable agreement with observations. At the uppermost model levels the attenuation in E39C-A is stronger than in E39C or observed. This might be related to a diagnostic artefact caused by the low coverage of the model grid by Lagrangian air parcels near the model top, leading to an artificial smoothing of the diagnostic output (see Sect. 2.2). In view of the phase propagation the upgraded model version E39C-A is in very good agreement with HALOE observations, indicating a significant improvement in the simulated tropical ascent compared to E39C. On the one hand, this result is associated with a reduced vertical diffusion of the Lagrangian scheme (Stenke et al., 2007). On the other hand, the tropical upward mass flux in E39C-A is approximately 25% lower than in E39C, which is in better agreement with observations. E39C overestimates the tropical upward mass flux at 100 hPa, with values of 19.4×10^9 kg/s (DJF) and 16.4×10^9 kg/s (JJA), by a factor of about 1.5 compared to observations and middle atmosphere models (Grewe, 2006). This slowdown of the tropical ascent in E39C-A is related to a decreased wave forcing on the mean meridional circulation as discussed in Sect. 3.1.

3.2.2 Stratospheric methane

The stratospheric methane concentration is mainly controlled by two processes: Transport and oxidation of methane which primarily occurs in the middle and upper stratosphere. Assuming that the methane oxidation is adequately captured in the models, methane is often regarded as a suitable transport tracer, especially for downward motion inside the polar vortices.

ACPD
8, 18727–18764, 2008

Figure 5 shows the zonal mean CH_4 mixing ratio at 50 hPa from E39C, E39C-A and HALOE for October in order to examine the isolated descent inside the Antarctic vortex. In extra-tropical regions the methane mixing ratios from E39C are remarkably higher than observed, despite a reasonable performance in tropical regions. Eyring et al. (2006) attributed this deficiency mainly to modelled transport. As previous results with ATTILA indicate advancements in modelled dynamics and transport (Reithmeier and Sausen, 2002; Stenke et al., 2007), one might expect that ATTILA also leads to an improved methane distribution in E39C-A. However, E39C-A shows a similar performance as E39C, i.e. a good agreement with HALOE observations in the tropics and a clear overestimation of observed methane concentrations in the extra-tropics. The results for the Northern Hemisphere spring time (March) are similar and therefore not shown. The underestimation of the meridional methane gradient at 50 hPa could have several reasons: A too weak descent inside the polar vortex and/or transport barrier at the vortex edge (see also Hein et al., 2001), or other drawbacks due to the model top centred at 10 hPa and a low vertical resolution above 25 km.

As mentioned above the oxidation of methane acts as a stratospheric sink. Consequently, air with low values of methane is transported downwards in polar regions with the Brewer-Dobson circulation. In both model version, E39C and E39C-A, oxidation of methane is considered, but since the model top layer is centred at 10 hPa the main fraction of the methane oxidation occurring in the middle and upper stratosphere is not captured which contributes to the simulated methane excess.

Reithmeier et al. (2008) have already pointed out that the edge of the polar vortex acts as a very efficient transport barrier in the model. In order to further unravel the other effects, sensitivity simulations have been performed including an upper boundary condition for methane: At 10 hPa the observed (HALOE) horizontal methane gradient is prescribed. The normalised meridional gradient is then multiplied with the actual simulated methane mixing ratio in the tropics to receive the upper boundary condition. The results of these sensitivity simulations are also included in Fig. 5 (indicated as “with UB”). Including an upper boundary for methane E39C-A is in much better

ACPD
8, 18727–18764, 2008

agreement with HALOE observations, especially in the Northern Hemisphere. In polar regions of the Southern Hemisphere the simulated methane values are about 0.3–0.4 ppmv (approx. 25%) lower than in the model version without upper boundary, but the model results still exceed the observations by about 0.3 ppmv. Nevertheless, the simulated methane bias is reduced by 50%. In case of E39C the consideration of an upper boundary for methane leads to a reduction of the simulated methane excess in northern extra-tropics, comparable to E39C-A. In southern high latitudes, however, the improvement in E39C is only marginal. For March (not shown) the sensitivity simulations reveal similar results: In the summer (southern) hemisphere both models show a reduced methane bias, while in northern high latitudes only the results from E39C-A indicate a clear improvement.

The underestimated methane sink clearly contributes to the simulated methane excess in the extra-tropical lower stratosphere. In case of the semi-Lagrangian transport scheme (E39C) the effect of the upper boundary condition is counteracted by too strong horizontal mixing across the vortex edge due to enhanced numerical diffusion, while ATTILA maintains steeper gradients and therefore better represents the polar barrier. The remaining methane excess in E39C-A suggests that the simulated descent inside the polar vortices is not strong enough which may be regarded as an effect of the low upper boundary (see also Hein et al., 2001).

3.3 Tracer distributions

In this section we examine the implications of the Lagrangian transport for simulated tracer distributions with a focus on ozone and ozone-relevant trace species. First, the distribution of inorganic chlorine (Cl_y) in the Southern Hemisphere polar spring is analysed, since stratospheric chlorine acts as a key driver for ozone depletion.

3.3.1 Inorganic chlorine (Cl_y)

Figure 6 (left) shows the climatological mean Cl_y profile at 80° S for October. The vertical Cl_y profile provides information to which extent air masses from the upper stratosphere (high Cl_y values) descent inside the polar vortex without horizontal mixing across the vortex edge. In E39C polar Cl_y (Fig. 6, left) and HCl (not shown, see Fig. 11 in Eyring et al., 2006) profiles are generally shifted upwards which leads to an underestimation of the Cl_y and HCl concentrations at lower stratospheric levels. As a consequence E39C also simulates an unrealistic ozone hole profile in the Antarctic stratosphere (Hein et al., 2001; Eyring et al., 2006, see Sect. 3.3.2).

Consistent with the findings of the previous section, the Lagrangian transport in E39C-A leads to a significant improvement with regard to the simulated Cl_y profile. Compared to E39C high stratospheric Cl_y concentrations extend further downward in E39C-A which is in good agreement with the simulated profiles of the majority of CCMs (grey lines in Fig. 6). This result holds also for the simulated HCl distribution (not shown): HCl at lower stratospheric levels (50 hPa) is significantly higher than in E39C and agrees well with HALOE observations.

For reliable simulations of the temporal evolution of ozone and ozone recovery, it is important to reproduce not only the mean Cl_y distribution, but also the temporal evolution of the stratospheric Cl_y concentrations in response to the increasing CFC loading. Figure 6 (right) shows the time series of Cl_y in the Antarctic lower stratosphere in October. Though E39C simulates a Cl_y increase during the 1980s and 1990s, the simulated Cl_y values are generally too low and the rate of increase is too weak. In contrast E39C-A shows much higher peak Cl_y values of around 3 ppbv during the second half of the 1990s. After 2000 the model simulates a beginning decrease of the stratospheric Cl_y which is consistent with the prescribed Cl_y upper boundary condition. In 2004 E39C-A simulates a mean Cl_y value of around 2.6 ppbv, while Aura MLS HCl measurements indicate a value of 3.3 ppbv. However, as already discussed in Eyring et al. (2006) there are large uncertainties of 10 to 15% in these values because of the limited data

ACPD
8, 18727–18764, 2008

available and possible biases in HCl measurements.

In E39C (and E39C-A) the photolysis of organic chlorine species in the upper stratosphere is considered by an upper boundary condition for Cl_y (see Sect. 2.2). However, in E39C the information about the Cl_y content provided at the model top does not penetrate into the lower stratosphere. This suggests that the strong numerical diffusion of the semi-Lagrangian transport scheme in E39C leads to an artificial "counter-gradient-transport" in case of low vertical resolution and large tracer gradients (Rasch and Lawrence, 1998; Grewe et al., 2002) resulting in an upward shift of the vertical tracer profiles. Furthermore, the considerable numerical diffusion of the semi-Lagrangian scheme also leads to a flattening of meridional tracer gradients (Reithmeier and Sausen, 2002; Stenke et al., 2007), e.g. at the vortex edge, which is not the case in the numerically non-diffusive advection scheme ATTILA.

3.3.2 Ozone

To show the direct and indirect impacts of ATTILA on the ozone distribution, a selection of ozone profiles from E39C, E39C-A and radiosonde observations are compared in Fig. 7. The observations are taken from the Binary DataBase of Profiles (BDBP), a new database of high vertical resolution measurements (Hassler et al., 2008). One main improvement of using ATTILA on the ozone profiles is a better representation of the ozonopause, i.e. the transition of low ozone concentrations in the troposphere to higher concentrations representative for the stratosphere. While in E39C this transition occurs at too high altitudes, E39C-A shows a much better agreement with observations. This effect is most evident at high latitudes (see Fig. 7), where the deviations of E39C from observations are largest (see Fig. 9 in Hein et al., 2001), but also at middle and low latitudes the simulation of the transition of ozone between troposphere and stratosphere is improved in E39C-A (not shown). One of the reasons for the downward shift of the ozonopause is certainly the improved representation of the tropopause in E39C-A (Sect. 3.1).

The maximum in ozone partial pressure in the stratosphere, which is generally over-

estimated in E39C (cp. Fig. 9 in Hein et al., 2001), is still too high in E39C-A. However, the deviation is slightly reduced in E39C-A for northern high latitudes (Fig. 7 left) and for mid-latitudes (not shown). In southern high latitudes the situation is different in that E39C-A shows even higher values of ozone than E39C at all altitudes in winter (Fig. 7 right) and spring (Fig. 8 left). Note that in E39C, the southern high latitudes are the only region where ozone is not overestimated. This is caused by a compensation of errors, i.e. the strong cold bias in this region counteracts the underestimated Cl_y concentrations. Since the cold bias is significantly reduced (Sect. 3.1) and the Cl_y values are much more realistic in E39C-A (Sect. 3.3.1), ozone levels in southern polar regions are higher, being consistent with the general overestimation of total ozone in the model.

As discussed in the last section, the profiles of Cl_y and HCl are shifted upward in E39C. This causes the depletion of polar ozone to occur at too high levels in E39C. This is evident in Fig. 8 (left) where a typical year with a disturbed ozone profile is shown for E39C and E39C-A. The unrealistic minimum in ozone concentrations in E39C at around 30 hPa due to excessive Cl_y values in this region is not longer apparent in E39C-A. This is shown more clearly in the right panel of Fig. 8 by the relative anomaly of ozone concentrations for the perturbed conditions of the 1990s. The level of maximal ozone reduction is shifted downward from about 30 hPa to about 50 hPa, being consistent with the downward shift of the Cl_y profile (see Fig. 6). In addition, the region of ozone depletion spans over a wider range of height levels in E39C-A.

Not only the spatial but also the temporal evolution of ozone is influenced by the use of ATTILA. Even though ozone values are generally higher in the south polar region in E39C-A (see discussion above), the strong negative trend in total column ozone in spring (September to November) is greater in magnitude in E39C-A both for absolute (see Fig. 9) and relative anomalies (the trends correspond to −8% and −12% per decade for E39C and E39C-A, respectively). This increase in the trend is consistent with changes in the Cl_y temporal evolution (Fig. 6). Since E39C is underestimating the loss in total column ozone (cp. Fig. 15b in Eyring et al., 2006) the changes brought upon by ATTILA are a clear improvement towards a more realistic simulation of the

ACPD
8, 18727–18764, 2008

evolution of atmospheric ozone.

4 Conclusions

In this paper we have presented the E39C-A model, an upgraded version of the coupled chemistry-climate model (CCM) E39C using the purely Lagrangian scheme ATTILA for tracer transport instead of the operational semi-Lagrangian scheme. Stratospheric model dynamics and simulated distributions of several trace species have been evaluated against observations and former model results in order to assess the implications of the Lagrangian advection scheme for the results of chemistry-climate simulations.

So far Lagrangian methods have been used for passive tracer transport (e.g. Reithmeier and Sausen, 2002) or in chemistry transport models (CTMs) (e.g. McKenna et al., 2002a,b). Recently, Stenke et al. (2007) successfully applied the Lagrangian scheme ATTILA for the transport of active trace species, i.e. water vapour and cloud water, in the GCM E39. The present study is the first time that a Lagrangian advection scheme is used in a fully coupled CCM.

The Lagrangian method has the advantage that it is strictly mass conserving and numerically non-diffusive. In general, ATTILA is able to maintain steeper and more realistic tracer gradients than the operational semi-Lagrangian scheme. In case of water vapour, ATTILA shows a steeper meridional gradient at the subtropical tropopause and a remarkably reduced water vapour content in the extra-tropical lowermost stratosphere, leading to much better agreement with observations. Due to changes in the radiative heating rates, also modelled temperatures benefit from the advanced numerical characteristics of the Lagrangian algorithm, i.e. the simulated cold bias is reduced to one third of its original value. In response to the reduced wet and cold bias in the extra-tropical lowermost stratosphere, model dynamics show several improvements: The mean zonal wind fields are more realistically reproduced, especially the observed wind reversal in the stratosphere below 10 hPa is now adequately simulated in E39C-A. Resulting changes in wave propagation and dissipation lead to a weakening of the

simulated mean meridional circulation and therefore a more realistic representation of tropical upwelling. In turn, the mentioned upgrades in model dynamics are reflected in simulated tracer distributions, e.g. in the atmospheric tape recorder signal or the representation of the ozonopause. Thus, several model deficiencies in E39C originate from a simulated moisture bias caused by the exceptional high numerical diffusion of the operational semi-Lagrangian advection scheme.

Furthermore, Lagrangian transport and its implications for simulated tracer distributions and model dynamics have an impact on modelled chemistry. For example, the simulated distribution of inorganic chlorine (Cl_y) is crucial for the simulation of stratospheric ozone depletion. ATTILA leads to a downward shift of the polar Cl_y profile in E39C-A, and therefore higher and more realistic Cl_y values in the lower stratosphere. Consequently the level of maximum ozone depletion is shifted downward from 30 hPa to 50 hPa. Furthermore, the simulated Cl_y trend in the lower stratosphere, which is underestimated in E39C, is realistically reproduced in E39C-A. In response to the improved Cl_y trend E39C-A shows a more realistic representation of the temporal evolution of atmospheric ozone. Hence, numerical limitations of the applied advection scheme may not only affect mean spatial tracer distributions, but also the simulation of their long-term development.

Assuming that all relevant source and sink processes are adequately captured in the models, long-lived tracers like methane or nitrous oxide are commonly used to evaluate stratospheric transport characteristics. However, model deficiencies with respect to those source and sink processes may lead to misinterpretations of the tracer diagnostics. In our case a large fraction of the simulated methane excess in the extra-tropical lower stratosphere is related to an underestimation of the stratospheric methane oxidation due to the low model top, and not to stratospheric transport problems as suggested by Eyring et al. (2006). Additional model simulations including an upper boundary condition for methane provide further insights into the stratospheric transport characteristics of the model. The sensitivity of the methane distribution to the representation of the stratospheric methane sink calls for caution in using simulated tracer distributions

as a diagnostic of the large-scale circulation without further reflection.

Model deficiencies might have different reasons which certainly differ among the models. In previous studies the position of the upper boundary has been widely discussed as a potential reason for model biases in E39C (e.g. Hein et al., 2001; Austin et al., 2003; Eyring et al., 2006). The study of Stenke et al. (2007) and the present work have shown that many deficiencies in E39C are not caused by the low model top, but primarily by the exceptional high numerical diffusion of the semi-Lagrangian advection scheme and resultant model biases in the distributions of radiatively active trace species which feed back to model dynamics. However, Lagrangian transport can not be regarded as an universal remedy for all kind of model deficiencies. For example, E39C-A still shows a low temperature bias in the polar stratosphere above 50 hPa in winter, the so-called "cold pole" problem. Nevertheless, replacing the operational semi-Lagrangian scheme in E39C with ATTILA was an important step towards improved model projections.

Acknowledgements. We especially thank R. Sausen for supporting the Lagrangian modelling activities in our group and for many constructive discussions. We are also grateful to M. Ponater for his helpful comments on the manuscript. Special thanks go to B. Hassler for providing the ozonesonde profiles shown in Fig. 7, J.-U. Grooß for providing the HALOE water vapour climatology and P. Newman for providing the NCEP/NCAR heat flux data. ECMWF ERA-40 data used in this study have been obtained from the ECMWF data server. This study was supported by the European Commission through the projects SCOUT-O3 and HISAC under the 6th Framework Programme and by the German Research Foundation (DFG) through the priority programme MetStröm. Parts of the model simulations have been performed on the NEC SX-6 high performance computer of the German Climate Computing Centre (DKRZ) Hamburg.

References

Atherton, C. A., Grotch, S., Parrish, D. D., Penner, J. E., and Walton, J. J.: The role of anthropogenic emissions of NOx on tropospheric ozone over the North Atlantic Ocean: A three dimensional, global model study, Atmos. Environ., 30, 1739–1749, 1996. 18731

Austin, J., Shindell, D., Beagley, S. R., Brühl, C., Dameris, M., Manzini, E., Nagashima, T., Newman, P., Pawson, S., Pitari, G., Rozanov, E., Schnadt, C., and Shepherd, T. G.: Uncertainties and assessments of chemistry-climate models of the stratosphere, Atmos. Chem. Phys., 3, 1–27, 2003, http://www.atmos-chem-phys.net/3/1/2003/. 18729, 18749

Brühl, C. and Crutzen, P. J.: MPIC two-dimensional model, in: The atmospheric effects of stratospheric aircraft: Report of the 1992 models and measurement workshop, edited by: Prather, M. and Remsberg, E., NASA Reference Publ. 1292, 703–706, Washington, D.C., 1993. 18736

Collins, W. J., Stevenson, D. S., Johnson, C. E., and Derwent, R. G.: The European regional ozone distribution and its links with the global scale for the years 1992 and 2015, Atmos. Environ., 34, 255–267, 2000. 18731

Dameris, M., Grewe, V., Ponater, M., Deckert, R., Eyring, V., Mager, F., Matthes, S., Schnadt, C., Stenke, A., Steil, B., Brühl, C., and Giorgetta, M. A.: Long-term changes and variability in a transient simulation with a chemistry-climate model employing realistic forcing, Atmos. Chem. Phys., 5, 2121–2145, 2005, http://www.atmos-chem-phys.net/5/2121/2005/. 18729, 18730, 18732, 18734, 18735, 18736, 18737

Dameris, M., Matthes, S., Deckert, R., Grewe, V., and Ponater, M.: Solar cycle effect delays onset of ozone recovery, Geophys. Res. Lett., 33, L03806-1–L03806-4, doi:10.1029/2005GL024741, 2006. 18732

Edmon, H. J., Hoskins, B. J., and McIntyre, M. E.: Eliassen-Palm cross sections for the troposphere, J. Atmos. Sci., 37, 2600–2616, 1980. 18738

Eluszkiewicz, J., Helmer, R. S., Mahlman, J. D., Bruhwiler, L., and Takacs, L. L.: Sensitivity of Age-of-Air calculations to the choice of advection scheme, J. Atmos. Sci., 57, 3185–3201, 2000. 18731, 18733

Eyring, V., Butchart, N., Waugh, D., Akiyoshi, H., Austin, J., Bekki, S., Bodeker, G., Boville, B., Brühl, C., Chipperfield, M., Cordero, E., Dameris, M., Deushi, M., Fioletov, V., Frith, S., Garcia, R., Gettelman, A., Giorgetta, M., Grewe, V., Jourdain, L., Kinnison, D., Mancini, E., Manzini, E., Marchand, M., Marsh, D., Nagashima, T., Newman, P., Nielsen, J., Pawson, S., Pitari, G., Plummer, D., Rozanov, E., Schraner, M., Shepherd, T., Shibata, K., Stolarski, R., Struthers, H., Tian, W., and Yoshiki, M.: Assessment of temperature, trace species, and ozone in chemistry-climate model simulations of the recent past, J. Geophys. Res., 111,

D22308, doi:10.1029/2006JD007327, 2006. 18729, 18731, 18739, 18740, 18742, 18744, 18746, 18748, 18749, 18761

Gates, W. L., Boyle, J. S., Covey, C., Dease, C. G., Doutriaux, C. M., Drach, R. S., Fiorino, M., Glecker, P. J., Hnilo, J. J., Marlais, S. M., Phillips, T. J., Potter, G. L., Santer, B. D., Sperber, K. R., Taylor, K. E., and Williams, D. N.: An overview of the results of the Atmospheric Model Intercomparison Project (AMIP I), B. Am. Meteorol. Soc., 80, 29–55, 1999. 18729

Giorgetta, M. A. and Bengtsson, L.: Potential role of the quasi-biennial oscillation in the stratosphere-troposphere exchange as found in water vapor in general circulation model experiments, J. Geophys. Res., 104, 6003–6019, 1999. 18735

Grewe, V.: The origin of ozone, Atmos. Chem. Phys., 6, 1495–1511, 2006, http://www.atmos-chem-phys.net/6/1495/2006/. 18741

Grewe, V.: Impact of climate variability on tropospheric ozone, Sci. Total Environ., 374, 167–181, 2007. 18732

Grewe, V., Brunner, D., Dameris, M., Grenfell, J. L., Hein, R., Shindell, D., and Staehelin, J.: Origin and variability of upper tropospheric nitrogen oxides and ozone at northern mid-latitudes, Atmos. Environ., 35, 3421–3433, 2001. 18733

Grewe, V., Dameris, M., Fichter, C., and Sausen, R.: Impact of aircraft NO_x emissions. Part 1: Interactively coupled climate-chemistry simulations and sensitivities to climate-chemistry feedback, lightning and model resolution, Meteorol. Z., 3, 177–186, 2002. 18745

Grewe, V., Shindell, D. T., and Eyring, V.: The impact of horizontal transport on the chemical composition in the tropopause region: Lightning NO_x and streamers, Adv. Space Res., 33, 1058–1061, 2004. 18732

Grooß, J.-U. and Russell III, J. M.: Technical note: A stratospheric climatology for O_3, H_2O, CH_4, NO_x, HCl and HF derived from HALOE measurements, Atmos. Chem. Phys., 5, 2797–2807, 2005, http://www.atmos-chem-phys.net/5/2797/2005/. 18740

Hansen, J., Sato, M., Nazarenko, L., Ruedy, R., Lacis, A., Koch, D., Tegen, I., Hall, T., Shindell, D., Santer, B., Stone, P., Novakov, T., Thomason, L., Wang, R., Wang, Y., Jacob, D., Hollandsworth, S., Bishop, L., Logan, J., Thompson, A., Stolarski, R., Lean, J., Willson, R., Levitus, S., Antonov, J., Rayner, N., Parker, D., and Christy, J.: Climate forcings in Goddard Institute for Space Studies SI2000 simulations, J. Geophys. Res., 107, 4347, doi:10.1029/2001JD001143, 2002. 18735

Hassler, B., Bodeker, G. E., and Dameris, M.: Technical Note: A new global database of trace

gases and aerosols from multiple sources of high vertical resolution measurements, Atmos. Chem. Phys., 8, 5403–5421, 2008, http://www.atmos-chem-phys.net/8/5403/2008/. 18745

Haynes, P. H., Marks, C. J., McIntyre, M. E., Shepherd, T. G., and Shine, K. P.: On the downward control of extratropical diabatic circulations by eddy-induced mean zonal forces, J. Atmos. Sci., 48, 651–679, 1991. 18738

Hein, R., Crutzen, P. J., and Heimann, M.: An inverse modeling approach to investigate the global atmospheric methane cycle, Global Biogeochem. Cy., 11, 43–76, 1997. 18736

Hein, R., Dameris, M., Schnadt, C., Land, C., Grewe, V., Köhler, I., Ponater, M., Sausen, R., Steil, B., Landgraf, J., and Brühl, C.: Results of an interactively coupled atmospheric chemistry – general circulation model: Comparison with observations, Ann. Geophys., 19, 435–457, 2001, http://www.ann-geophys.net/19/435/2001/. 18732, 18742, 18743, 18744, 18745, 18746, 18749

Hitchman, M. and Huesmann, A.: A seasonal Climatology of Rossby Wave Breaking in the 320–2000-K Layer, J. Atmos. Sci., 64, 1922–1940, 2007. 18739

IPCC: Climate Change 2001 – The scientific basis, Intergovernmental Panel on Climate Change, Cambridge University Press, New York, USA, 2001. 18736

Jackman, C. H., Fleming, E. L., Chandra, S., Considine, D. B., and Rosenfield, J. E.: Past, present, and future modeled ozone trends with comparisons to observed trends, J. Geophys. Res., 101, 28 753–28 768, 1996. 18735

Kirchner, I., Stenchikov, G. L., Graf, H.-F., Robock, A., and Antuña, J. C.: Climate Model simulation of winter warming and summer cooling following the 1991 Mount Pinatubo volcanic eruption, J. Geophys. Res., 104, 19 039–19 055, 1999. 18735

Lamago, D., Dameris, M., Schnadt, C., Eyring, V., and Brühl, C.: Impact of large solar zenith angles on lower stratospheric dynamical and chemical processes in a coupled chemistry-climate model, Atmos. Chem. Phys., 3, 1981–1990, 2003, http://www.atmos-chem-phys.net/3/1981/2003/. 18733

Land, C., Feichter, J., and Sausen, R.: Impact of vertical resolution on the transport of passive tracers in the ECHAM4 model, Tellus (B), 54, 344–360, 2002. 18730, 18732, 18733

Lean, J., Rottmann, G., Kyle, H., Woods, T., Hickey, J., and Puga, L.: Detection and parameterisation of variations in solar mid- and near-ultraviolet radiation (22–400 nm), J. Geophys. Res., 102, 29 939–29 956, 1997. 18736

McKenna, D. S., Grooß, J.-U., Günther, G., Konopka, P., Müller, R., Carver, G., and Sasano, Y.: A new Chemical Lagrangian Model of the Stratosphere (CLAMS): 2. Formulation of chemistry scheme and initialization, J. Geophys. Res., 107, 4256, doi:10.1029/2000JD000113, 2002a. 18731, 18747

McKenna, D. S., Konopka, P., Grooß, J.-U., Günther, G., Müller, R., Spang, R., Offermann, D., and Orsolini, Y.: A new Chemical Lagrangian Model of the Stratosphere (CLAMS): 1. Formulation of advection and mixing, J. Geophys. Res., 107, 4309, doi:10.1029/2000JD000114, 2002b. 18731, 18747

Mote, P. W., Rosenlof, K. H., McIntyre, M. E., Carr, E. S., Gille, J. C., Holton, J. R., Kinnersley, J. S., Pumphrey, H. C., Russell III, J. M., and Waters, J. W.: An Atmospheric Tape Recorder: The Imprint of Tropical Tropopause Temperatures on Stratospheric Water Vapor, J. Geophys. Res., 101, 3989–4066, 1996. 18740

Newman, P., Nash, E., and Rosenfield, J.: What controls the temperature of the Arctic stratosphere during the spring?, J. Geophys. Res., 106, 19 999–20 010, 2001. 18739

Park, J. H., Ko, M. K. W., Jackman, C. H., Plumb, R. A., Kaye, J. A., and Sage, K. H.: Models and Measurements Intercomparison 2, Tech. Rep. NASATM-1999-209554, NASA, 1999. 18729

Pawson, S., Kodera, K., Hamilton, K., Shepherd, T. G., Beagley, S. R., Boville, B., Farrara, J. D., Fairlie, T. D. A., Kitoh, A., Lahoz, W. A., Langematz, U., Manzini, E., Rind, D. H., Scaife, A. A., Shibata, K., Simon, P., Swinbank, R., Takacs, L., Wilson, R., Al-Saadi, J. A., Amodei, M., Chiba, M., Coy, L., de Grandpre, J., Eckman, R. S., Fiorino, M., Grose, W. L., Koide, H., Koshyk, J. N., Li, D., Lerner, J., Mahlman, J. D., McFarlane, N. A., Mechoso, C. R., Molod, A., O'Neill, A., Pierce, R. B., Randel, W. J., Rood, R. B., and Wu, F.: The GCM-reality intercomparison project of SPARC (GRIPS): scientific issues and initial results, B. Am. Meteorol. Soc., 81, 781–796, 2000. 18729

Rasch, P. J. and Lawrence, M.: Recent development in transport methods at NCAR, Report No. 265, Max-Planck-Institut für Meteorologie, Hamburg, 1998. 18745

Rasch, P. J. and Williamson, D. L.: Computational aspects of moisture transport in global models of the atmosphere, Q. J. Roy. Meteor. Soc., 116, 1071–1090, 1990. 18733

Rayner, N. A., Parker, D. E., Horton, E. B., Folland, C. K., Alexander, L. V., Rowell, D. P., Kent, E. C., and Kaplan, A.: Global Analyses of sea surface temperatures, sea ice, and night marine air temperature since the late nineteenth century, J. Geophys. Res., 108, 4407, doi:10.1029/2002JD002670, 2003. 18734

Reithmeier, C. and Sausen, R.: ATTILA: Atmospheric Tracer Transport in a Lagrangian Model,

Tellus (B), 54, 278–299, 2002. 18730, 18731, 18732, 18733, 18742, 18745, 18747
Reithmeier, C., Sausen, R., and Grewe, V.: Investigating lower stratospheric model transport: Lagrangian calculations of mean age and age spectra in the GCM ECHAM4, Clim. Dynam., 30, 225–238, 2008. 18733, 18742
RETRO: Emission data sets and methodologies for estimating emissions, Report from REanalysis of the TROpospheric chemical composition over the past 40 years, available at: http://retro.enes.org/reports/D1-6_final.pdf, 2007. 18736
Rex, M., Salawitch, R. J., Santee, M. L., Waters, J. W., Hoppel, K., and Bevilacqua, R.: On the unexplained stratospheric ozone losses during cold Arctic Januaries, Geophys. Res. Lett., 30, 1008, doi:10.1029/2002GL016008, 2003. 18732
Robinson, W. A.: The Application of the Quasi-Geostrophic Eliassen-Palm Flux to the Analysis of Stratospheric Data, J. Atmos. Sci., 43, 1017–1024, 1986. 18738
Roeckner, E., Arpe, K., Bengtsson, L., Christoph, M., Claussen, M., Dümenil, L., Esch, M., Giorgetta, M., Schlese, U., and Schulzweida, U.: The atmospheric general circulation model ECHAM-4: Model description and simulation of present-day climate, Report No. 218, Max-Planck-Institut für Meteorologie, Hamburg, 1996. 18730, 18732
Sato, M., Hansen, J. E., McCormick, M. P., and Pollack, J. B.: Stratospheric aerosol optical depths, 1850–1990, J. Geophys. Res., 98, 22 987–22 994, 1993. 18735
Schmidt, G. A., Ruedy, R., Hansen, J. E., Aleinov, I., N. Bell, M. B., Bauer, S., Cairns, B., Canuto, V., Cheng, Y., Genio, A. D., Faluvegi, G., Friend, A. D., Hall, T. M., Hu, Y., Kelley, M., Kiang, N. Y., Koch, D., Lacis, A. A., Lerner, J., Lo, K. K., Miller, R. L., Nazarenko, L., Oinas, V., Perlwitz, J., Perlwitz, J., Rind, D., Romanou, A., Russell, G. L., Sato, M., Shindell, D. T., Stone, P. H., Sun, S., Tausnev, N., Thresher, D., and Yao, M.-S.: Present-day atmospheric simulations using GISS Model E: Comparison to in situ, satellite, and reanalysis data, J. Climate, 19, 153–192, doi:10.1175/JCLI3612.1, 2006. 18735
Schnadt, C., Dameris, M., Ponater, M., Hein, R., Grewe, V., and Steil, B.: Interaction of atmospheric chemistry and climate and its impact on stratospheric ozone, Clim. Dynam., 17, 501–517, 2002. 18732
Steil, B., Dameris, M., Brühl, C., Crutzen, P. J., Grewe, V., Ponater, M., and Sausen, R.: Development of a chemistry module for GCMs: Development of a chemistry module for GCMs: first results of a multiannual integration, Ann. Geophys., 16, 205–228, 1998, http://www.ann-geophys.net/16/205/1998/. 18732
Stenke, A. and Grewe, V.: Simulation of stratospheric water vapor trends: impact on strato-

spheric ozone chemistry, Atmos. Chem. Phys., 5, 1257–1272, 2005, http://www.atmos-chem-phys.net/5/1257/2005/. 18732

Stenke, A., Grewe, V., and Ponater, M.: Lagrangian transport of water vapor and cloud water in the ECHAM4 GCM and its impact on the cold bias, Clim. Dynam., 31, 491–506, doi: 10.1007/s00382-007-0347-5, 2008. 18730, 18731, 18733, 18734, 18737, 18740, 18741, 18742, 18745, 18747, 18749

Uppala, S. M., Kållberg, P. W., Simmons, A. J., Andrae, U., Da Costa Bechtold, V., Fiorino, M., Gibson, J. K., Haseler, J., Hernandez, A., Kelly, G. A., Li, X., K, O., Saarinen, S., Sokka, N., Allan, R. P., Andersson, E., Arpe, K., Balmaseda, M. A., Beljaars, A. C. M., van de Berg, L., Bidlot, J., Bormann, N., Caires, S., Chevallier, F., Dethof, A., Dragosavac, M., Fisher, M., Fuentes, M., Hagemann, S., Hólm, E., Hoskins, B. J., Isaksen, L., Janssen, P. A. E. M., Jenne, R., McNally, A. P., Mahfouf, J.-F., Morcrette, J.-J., Rayner, N. A., Saunders, R. W., Simon, P., Sterl, A., Trenberth, K. E., Untch, A., Vasiljevic, D., Viterbo, P., and Woollen, J.: The ERA-40 re-analysis, Q. J. Roy. Meteor. Soc., 131, 2961–3012, 2005. 18737

Williamson, D. L. and Rasch, P. J.: Water vapor transport in the NCAR CCM2, Tellus (A), 46, 34–51, 1994. 18733

WMO: Scientific assessment of ozone depletion: 2002, Report No. 47, World Meteorological Organization, Genf, Schweiz, 2003. 18736

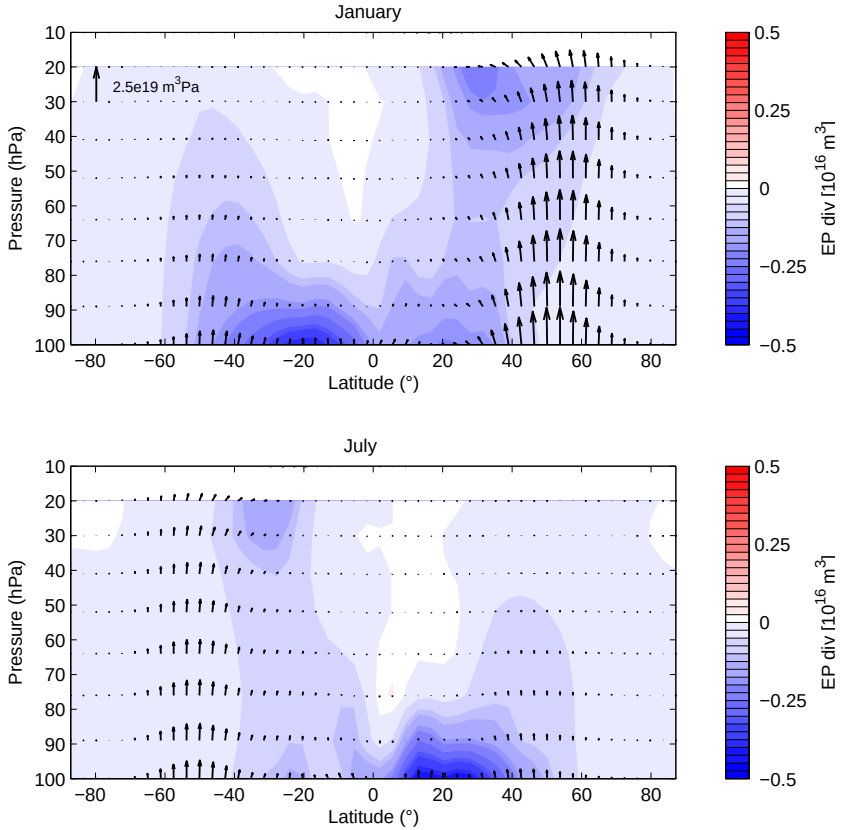

Fig. 1. January and July climatologies of EP fluxes (black arrows) and their divergences (coloured) over 40 years (1960–1999) calculated from E39C-A. Divergences are given in units of m^3 and fluxes in m^3 (horizontal component) and m^3 Pa (vertical component) due to weighting by mass (see text). The scale of the vertical flux is indicated in the upper left corner of the upper panel, a horizontal arrow of same length represents a flux of 0.436×10^{16} m^3.

ACPD
8, 18727–18764, 2008

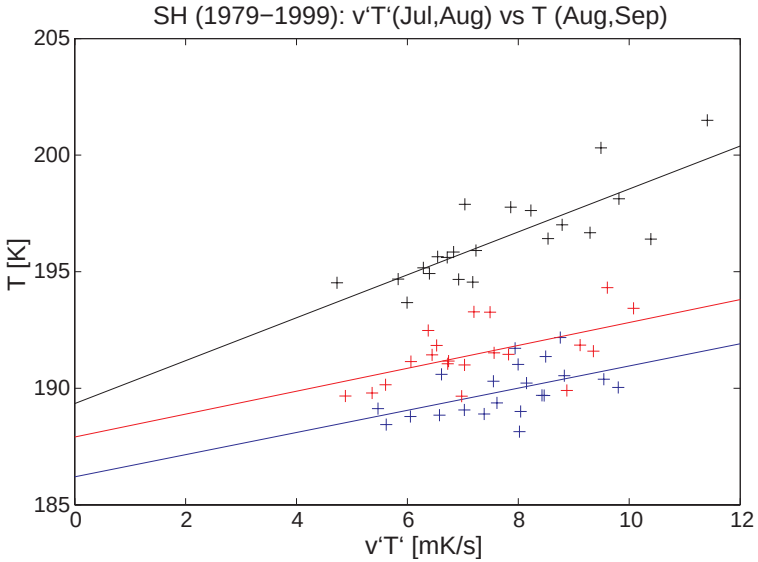

Fig. 2. Heat flux ($\overline{v'T'}$) at 100 hPa averaged over 40° S to 80° S for July and August versus temperature at 50 hPa averaged over 60° S to 90° S for August and September. Shown are 21 years from 1979 to 1999 for E39C (blue), E39C-A (red) and NCEP/NCAR reanalyses (black) together with their linear fits (solid lines). The slope of either model differs significantly from the observations at a 95% level.

ACPD
8, 18727–18764, 2008

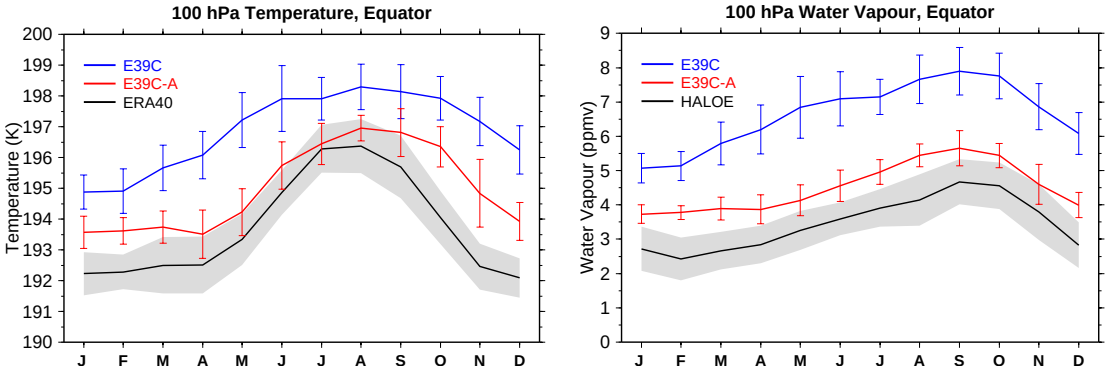

Fig. 3. Annual cycle of climatological mean temperature (left) and water vapour (right) at 100 hPa at the equator. Model results for the 1990s are compared to a temperature climatology derived from ERA-40 (1992–2001) and a HALOE water vapour climatology (1991–2002). The vertical bars and the grey shaded areas mark the standard deviation ($\pm 1\sigma$).

ACPD
8, 18727–18764, 2008

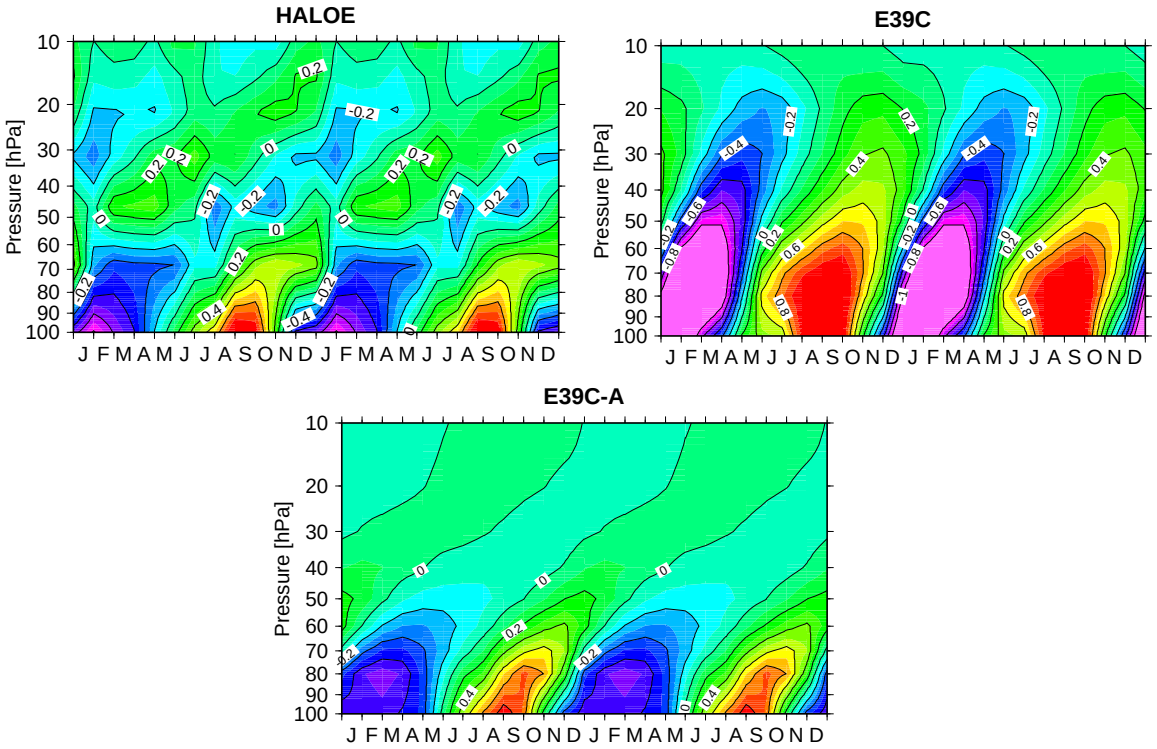

Fig. 4. Time-height sections of water vapour mixing ratio shown as the deviation [ppmv] from the mean profile, averaged between 10° N and 10° S ("atmospheric tape recorder") for HALOE observations (top left), E39C (top right) and E39C-A (bottom). Two consecutive cycles are shown.

ACPD
8, 18727–18764, 2008

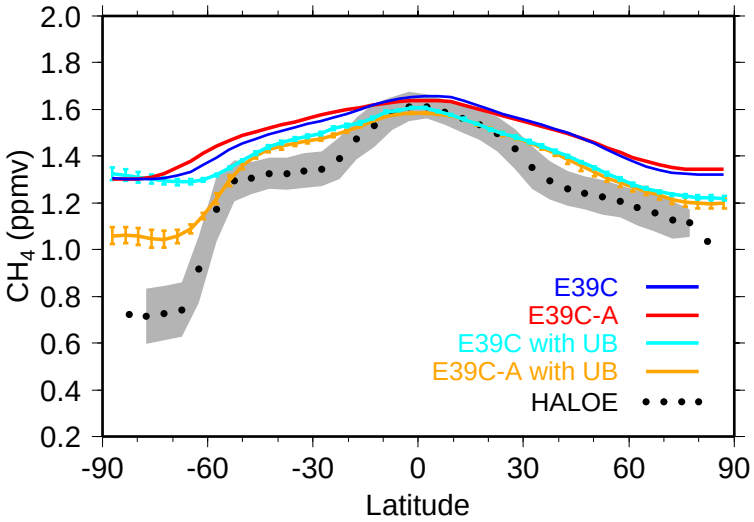

Fig. 5. Climatological zonal mean (1990 to 1999) CH_4 mixing ratios [ppmv] at 50 hPa in October for E39C (blue) and E39C-A (red). The results of the sensitivity simulations including an upper boundary condition for the methane gradient are shown in light blue (E39C) and orange (E39C-A) (the vertical bars indicate $\pm 1\sigma$). The grey area marks the HALOE standard deviation ($\pm 1\sigma$).

ACPD
8, 18727–18764, 2008

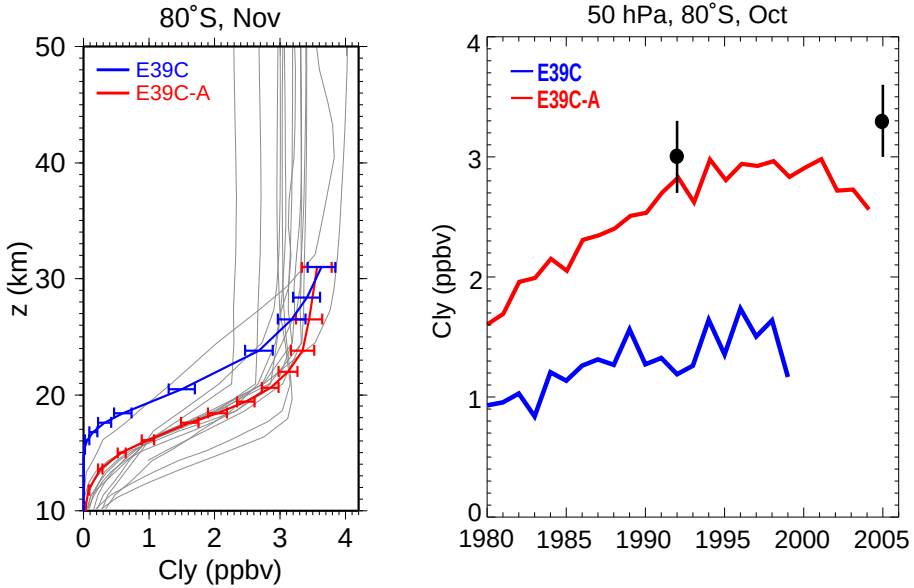

Fig. 6. Left: Climatological mean (1990 to 1999) vertical profiles at 80° S in November for Cl_y [ppbv] for E39C (blue) and E39C-A (red). The horizontal bars indicate the standard deviation ($\pm 1\sigma$). The grey lines show the results of all participating models from the intercomparison of Eyring et al. (2006, their Fig. 12a). Right: Times series of October mean Cl_y at 80° S, 50 hPa. Estimates of Cl_y from HALOE HCl measurements in 1992 and Aura MLS HCl in 2005 are shown as black signs. The values are taken from Eyring et al. (2006, their Fig. 12b).

ACPD
8, 18727–18764, 2008

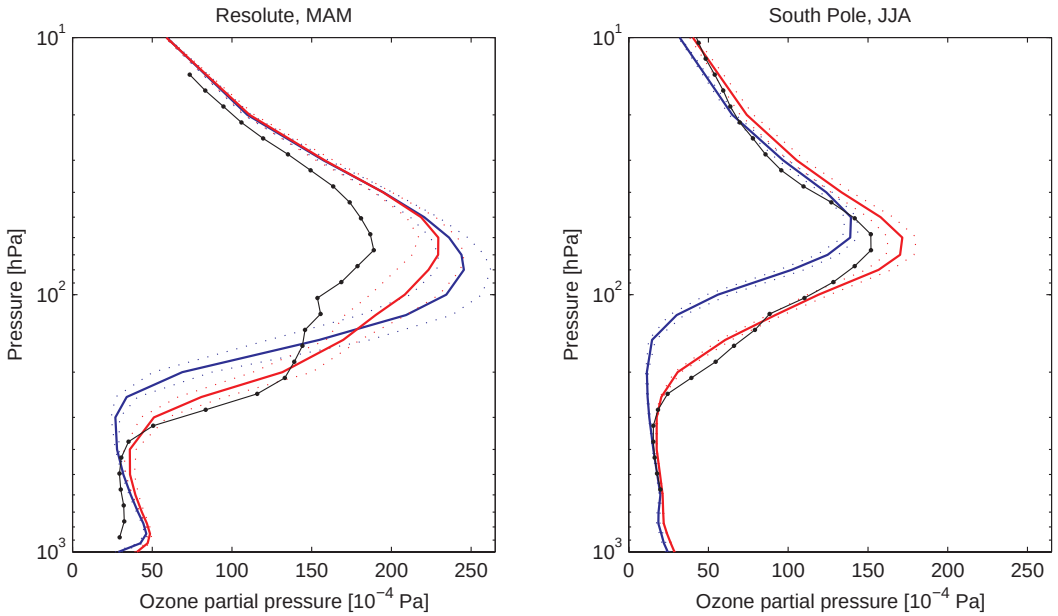

Fig. 7. Ozone partial pressure profiles for Resolute (74° N, 95° W) in spring (March–May, left panel) and for the South Pole in winter (June–August, right panel). Shown are means over 1983–1989 from E39C-A (red solid lines) and E39C (blue solid lines). Dotted lines indicate the standard deviation ($\pm 1\sigma$). Together with modelled ozone profiles, radiosonde observations are shown (black solid lines; observations are 1983–1989 averages for Resolute and 1986–1987 averages for the South Pole).

ACPD
8, 18727–18764, 2008

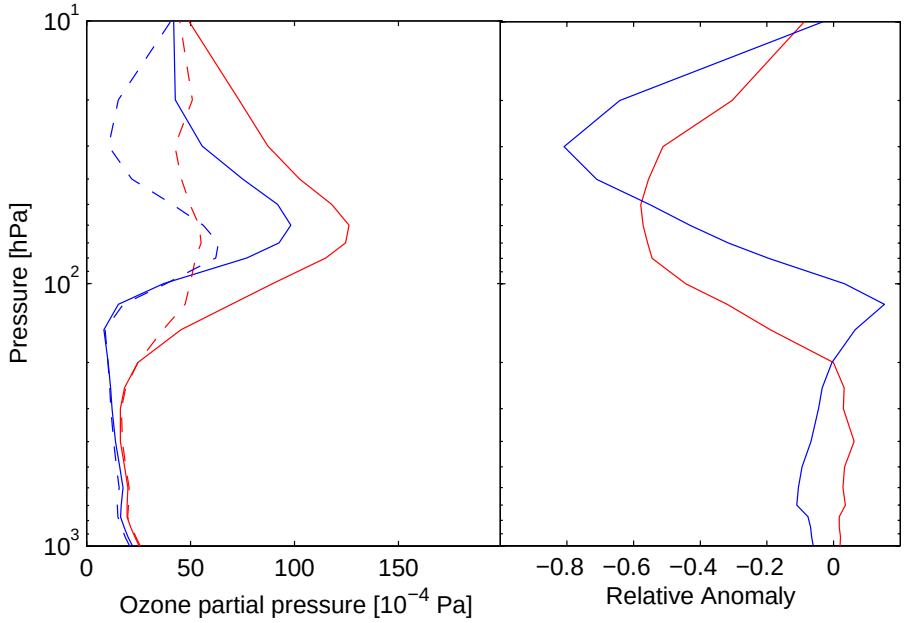

Fig. 8. Left: October mean profiles of ozone partial pressure for the South Pole for the early 1980s (solid lines; red: E39C-A, blue: E39C) and for one year in the 1990s representative for a disturbed ozone distribution (dashed lines; red: E39C-A, blue: E39C). Right: Relative difference in ozone partial pressure of the disturbed 1990s profile to the mean 1980s profile from the left panel ((mean-disturbed)/mean) for E39C (blue) and E39C-A (red).

ACPD
8, 18727–18764, 2008

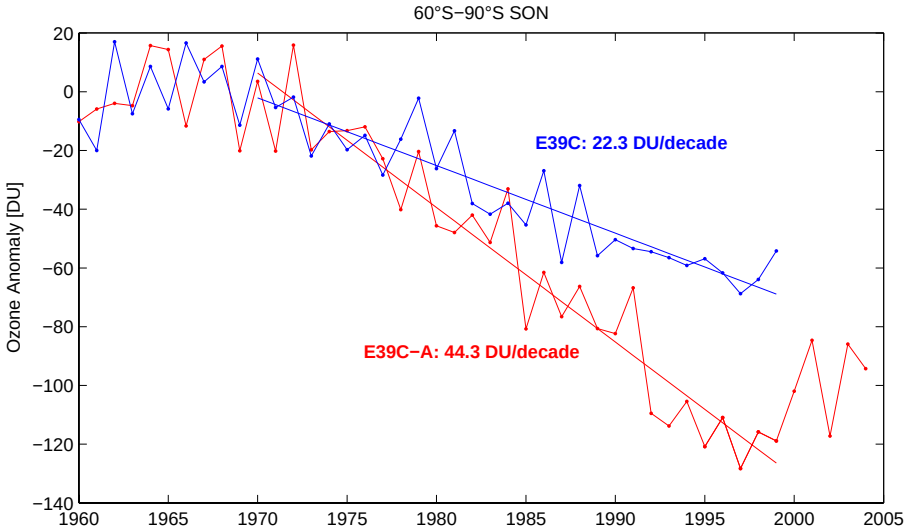

Fig. 9. Time series of total column ozone anomalies averaged over 60° S to 90° S and over September to November for E39C-A (red) and E39C (blue). The anomalies are calculated with respect to the 1960–1969 mean. Linear trends for the period 1970 to 1999 are added as solid lines together with their magnitude.

ACPD
8, 18727–18764, 2008